

pubs.acs.org/Macromolecules Article

Compositional and Temperature Dependence of Amorphous Polymer Networks Undergoing Mechanotropic Phase Transitions

Jeremy A. Herman, Jonathan D. Hoang, Joselle M. McCracken, and Timothy J. White*



Cite This: Macromolecules 2024, 57, 664-671



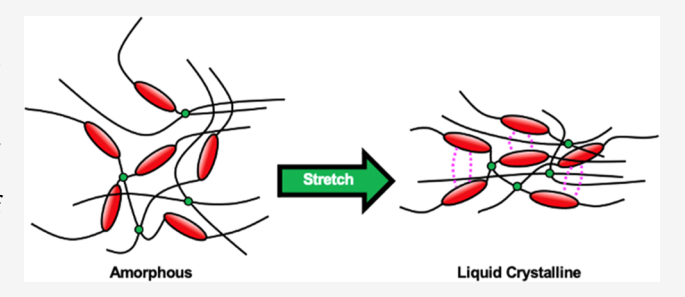
ACCESS I

III Metrics & More

Article Recommendations

Supporting Information

ABSTRACT: The deformation of liquid crystalline elastomers to load is nonlinear. Unlike traditional elastomeric thermosets, liquid crystalline elastomers can exhibit a slow recovery and considerable hysteresis. Recently, we reported the preparation of amorphous polymer networks that incorporate liquid crystalline monomer precursors. Upon deformation, these materials undergo mechanotropic phase transitions in which the initially amorphous state of the polymer network transitions into the nematic liquid crystalline phase. Perhaps unsurprisingly, the deformation of these materials is analogous to that of liquid crystalline elastomers. However, these



materials distinctly recover the amorphous state rapidly with limited hysteresis. Here, we explore the contribution of the liquid crystalline monomer concentration and temperature on the deformation of amorphous polymer networks that exhibit mechanotropic phase transitions. This investigation elucidates the nature of the mechanically induced phase transition in these amorphous polymer networks and identifies that mechanotropic phase transitions are thermotropic.

■ INTRODUCTION

Liquid crystalline elastomers (LCEs) are a unique class of polymer networks that are widely considered for functional use in optics, ^{1,2} soft robotics, ³ flexible electronics, ^{4,5} and health-care. ^{6,7} LCEs are typically lightly cross-linked polymer networks with glass transitions below room temperature that retain a liquid crystalline phase upon preparation. ⁸ The structural anisotropy is retained from liquid crystalline (e.g., mesogenic) monomer precursors. Considerable recent research has explored LCEs as soft, cyclable actuators that can be formulated to respond to a variety of external stimuli, including magnetic ^{9,10} and electrical fields ¹¹ as well as heat ^{12,13} and light. ^{14,15}

To realize directional actuation strain requires LCEs to be aligned. Several well-established processing approaches have been utilized¹⁶ to enforce monodomain alignment within LCEs. These include mechanical, 17,18 surface, 19,20 and rheological (such as that realized through direct ink write printing). 21,22 Here, we are concerned with another salient feature of LCEs and their analogues: nonlinear deformation and recovery. Prior examination of the deformation of unaligned and aligned LCE emphasizes that these materials are slow to recover and exhibit significant hysteresis.²³ Recently, we reported on a new class of liquid crystalline (LC)-based materials that deform nonlinearly but also rapidly recover with little hysteresis.²⁴ We refer to these as mechanotropic amorphous polymer networks (MT-APN) and these materials exhibit enhanced elastic recovery (40-70%) relative to traditional polydomain (PD-) LCEs. MT-APN have been shown to recover 100% of mechanically

induced strain in <60 s, whereas the analogous PD-LCE examined as a control experiment did not recover more than 68% at any time point. Contributing to this disparate mechanical recovery is that, unlike MT-APN, PD-LCE contain sufficient LC content that they possess a macroscopically unaligned LC phase defined by extensive intermolecular interactions. When mechanically stretched, the mesogen microdomains within PD-LCE contribute to nonlinear tensile responses that vary depending on whether the cross-linking temperature is below (nematic genesis, NG) or above (isotropic genesis, IG) the $T_{\rm NL}^{25-27}$ Consequently, not only can the deformation behavior of PD-LCE be impacted by thermal conditions but also can their orientational ordering and ultimately polymer network memory.

In contrast, the LC concentration in MT-APN is sufficiently low that the material is unable to retain or exhibit the LC phase upon preparation. While LC content reduction (inclusion of non-LC PEG comonomers, ²⁸ changes in chain extenders, ^{22,29,30} or new LC mesogens ^{31,32}) to study changes in material properties and actuation temperature has been reported elsewhere, MT-APN remain a distinct material class in which LC content is intentionally reduced beyond the

Received: September 13, 2023
Revised: December 20, 2023
Accepted: December 25, 2023
Published: January 9, 2024





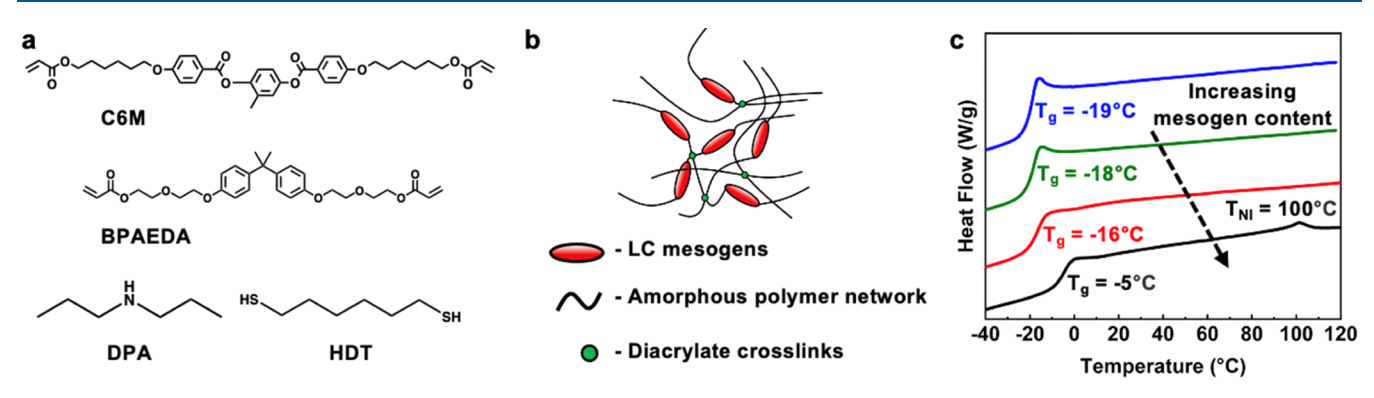


Figure 1. (a) Chemical structures of C6M and BPAEDA diacrylate monomers, base catalyst dipropylamine (DPA), and 1,6 hexanedithiol (HDT) used for thiol-Michael polymer preparation. (b) Schematic representing MT-APN containing diacrylate cross-links, large fractional amorphous content, and LC mesogens at concentrations too low to exhibit liquid crystalline properties. (c) Differential scanning calorimetry (DSC) traces for a series of thiol-Michael polymers containing different ratios of C6M/BPAEDA diacrylate content show slight increase in glass transition temperature (T_g) with LC content. Only the highest LC content (LCE-52, black trace) shows a nematic-to-isotropic transition temperature (T_{NI}) at 100°C.

threshold of LC phase retention. The absence of innate microdomain mesogen interactions in MT-APN minimizes the nonlinear and temperature-dependent mechanics that are seen in PD-LCE. It is only through the application of mechanical stress that the mesogens embedded in MT-APN begin to align in the direction of applied strain. We hypothesized in our previous work that, at high strains, the mesogens within MT-APN become sufficiently aligned that π - π stacking interactions develop into an LC phase within the network structure, causing these materials to undergo a mechanically induced phase change. While the data suggested this hypothesis to be true, it did not paint the complete picture to confirm a mechanically induced phase change was indeed occurring.

Mechanically induced phase changes have been reported elsewhere and have compelling implications for elastocaloric materials. Shape memory alloys³³⁻³⁵ (SMAs) and natural rubber³⁶⁻³⁸ are two widely studied and commercialized elastocaloric material types that depend on mechanically induced phase changes to function. In the case of SMAs, a mechanically induced first-order transition between the austenite and martensite phase generates a large temperature change (30°C) but requires significant input stress (~1 GPa).³³ Natural rubber exhibits a moderate temperature change (10°C) in response to very large strains (>500%) due to strain-induced crystallization of its polymer chains.³ Both of these materials are classified as elastocaloric because they undergo temperature changes that relate to shifts in their network order, and both materials rely on mechanical inputs to varying degrees to manifest a mechanical phase transition.

Similarly, mechanically induced phase transitions in MT-APN manifest compelling properties for use as functional materials such as for solid-state refrigeration³⁹ and dynamic optical films.⁴⁰ In addition to their excellent mechanical recovery from thermal cycling, MT-APN undergo very large changes in orientational ordering (orientation parameter > 0.3) in response to strain and are mechanically tougher than conventional APN of similar formulation (those comprising no LC content).²⁴ The mechanically induced phase transition from the amorphous to LC phase that is characteristic of MT-APN leads to an appreciable temperature increase (~2°C) at small strains (100%) and small stress input (1–2 MPa), making them competitive in this sense with natural rubber and SMAs. Ultralow hysteresis, high mechanical cyclability, enhanced elastic recovery, and appreciable temperature change

at small strains each make MT-APN particularly compelling for use as an elastocaloric material.

Here, we extend upon the prior study by investigating mechanotropic phase transitions in materials prepared by thiol-Michael reactions. Generally, this work seeks to confirm the nature of the mechanotropic phase transition and to confirm whether it is thermotropic or not. Toward this end, this examination explores compositions with a range of LC content and characterizes the deformation, orientational ordering, and actuation. In so doing, control examinations of LCEs in the polydomain orientation emphasize the similarity in mechanical deformation when these materials are heated about their $T_{\rm NI}$.

■ RESULTS AND DISCUSSION

Here, we are concerned with understanding the thermotropic nature of mechanotropic (MT) phase transitions in amorphous polymer networks (MT-APN). These materials are amorphous (isotropic) in an undeformed state. Upon deformation, these materials undergo a phase transition to form an LCE retaining the nematic phase. The deformation of these materials is accompanied by an elastocaloric temperature change.³⁹ The materials examined here are differentiated by their preparation state. Compositions that do not form a liquid crystal (LC) phase upon mixing or upon deformation will be referred to as APN-XX where XX is the concentration of the LC comonomer in mole percent. Compositions that do not form an LC phase upon preparation but undergo an MT phase transition were prepared with 32 mol% LC content and will be referred to as MT-APN-32. Compositions that retain the LC phase were prepared with 52 mol% LC content and referred to as LCE-52. Compositions APN-0 and APN-14 are utilized throughout this study to illustrate the deformation of similar, purely amorphous, elastomeric polymer networks.

All materials in this article were prepared by a two-stage reaction. First, the diacrylate monomers were oligomerized by thiol-Michael addition. Again, the polymer networks were prepared by varying the relative mole fraction of a classical liquid crystalline diacrylate (C6M) for bisphenol A ethoxyate diacrylate (BPAEDA). BPAEDA was selected as it is an aromatic but nonliquid crystalline diacrylate with a similar molecular weight to C6M. Chemical structures of the diacrylate monomers, thiol, and base catalyst are given in Figure 1a. The C6M/BPAEDA diacrylate monomer mixtures were oligomerized via thiol-Michael addition using a 1:0.85

acrylate-to-thiol mole ratio with hexanedithiol (HDT) as a chain extender and dipropylamine (DPA) as a base catalyst. The molar excess of acrylate functional groups in all formulations results in acrylate-terminated oligomers. The acrylate-terminated oligomers were subsequently cross-linked via photopolymerization. C6M mole fractions ranged from 0 to 52 mol% in the compositions examined here. The thiol content was constant in all formulations at 44 mol%. The formulation with 52 mol% C6M is a conventional LCE in the polydomain state (here, isotropic genesis), while the other formulations are amorphous upon preparation. At a threshold concentration, the MT-APN contains significant LC content but not enough to form an LC phase (illustrated in Figure 1b). The state (phase) of the polymer networks was characterized by differential scanning calorimetry (DSC, Figure 1c). All four materials are elastomeric at room temperature, with glass transition temperatures (T_g) increasing with the LC content $(T_{\sigma} < 22^{\circ}\text{C})$. Figure 1c confirms that only LCE-52 (Figure 1c, black trace) exhibited a second thermal transition characteristic of a nematic to isotropic transition in LCE ($T_{\rm NI}$ = 100°C, Table 1). The absence of a second transition (e.g., a $T_{\rm NI}$) for

Table 1. Mole Fraction (mol%), Glass Transition Temperature $(T_{\rm g})$, and Nematic-to-Isotropic Transition Temperature $(T_{\rm NI}$, When Applicable) for Thiol-Michael Materials

Sample	C6M (mol %)	$T_{\rm g}$ (°C)	$T_{\rm NI}$ (°C)
LCE-52	52	-5	100
MT-APN-32	32	-16	-
APN-14	14	-18	-
APN-0	0	-19	-

C6M/BPAEDA networks with \leq 32 mol% C6M is a strong indication that the materials are amorphous. Although our study focuses on compositions summarized in Table 1, other polymer networks were prepared with C6M concentrations between MT-APN-32 and LCE-52, such as LCE-39 (Figure S1).

These materials were then subject to deformation via tensile tests undertaken with dynamic mechanical analysis (DMA) to determine the stress—strain response of each material to failure (Figure 2a). As anticipated, LCE-52 exhibited three tensile regions characteristic of the deformation of an LCE transitioning from a polydomain to monodomain orientation.

These regions are referred to as the linear elastic (Figure 2a-1), soft elastic plateau (Figure 2a-2), and strain hardening (Figure 2a-3) regimes. The second regime, the soft elastic plateau, is characteristic of LCEs and is associated with the (re)-orientation of the liquid crystalline domains to the loading axis. At strain values exceeding 150% strain, the material transitions into a strain hardening (0.32 MPa/%) regime characterized by a rapid increase in stress with the applied strain. As evident in Figure 2a, the APN-0 exhibits only modest strain hardening (0.0076 MPa/%) typical of a traditional elastomeric polymer network.

The mechanical deformation of networks prepared with intermediate C6M concentrations displays tensile behavior similar to that of both LCE-52 and APN-0. Most evident in MT-APN-32, the deformation is typified by an extended linear response and does not exhibit a classical soft elastic plateau. The deformation of MT-APN-32 is soft but notably exhibits considerable strain hardening at approximately 150% strain. In comparing the deformation of MT-APN-32 to APN-14 and APN-0, strain hardening is strongly affected by the C6M concentration. The similarities in strain hardening response between LCE-52 and MT-APN-32 (0.32 and 0.26 MPa/%, respectively) may indicate that the mesogens in MT-APN-32 align to the direction of stretch.

To further understand the association of orientation and deformation, we monitored the deformation of the materials with wide-angle X-ray scattering (WAXS). Orientation parameters (S) were measured from WAXS patterns collected at 20% strain intervals for each material (Figure S2). As evident in Figure 2b, the association of deformation and orientation parameters is strongly dependent on composition. Notably, the orientation of LCE-52 is 0 at 0% strain, as this sample is polydomain and the beamwidth of the incident X-ray is much larger than the domain size. Incorporating C6M into the MT-APN-32 and APN-14 networks distinguishes the measurements from APN-0. The relative degree of orientation as well as the strength of coupling increases with further increase in C6M concentration. WAXS patterns at the final deformation of each material are presented in Figure 2c. LCE-52 achieves the highest orientation parameter upon deformation. For MT-APN samples with comparatively high concentrations of C6M, we propose that the deformation of the material aligns the mesogenic units, which can then associate via intermolecular interaction, strengthening the

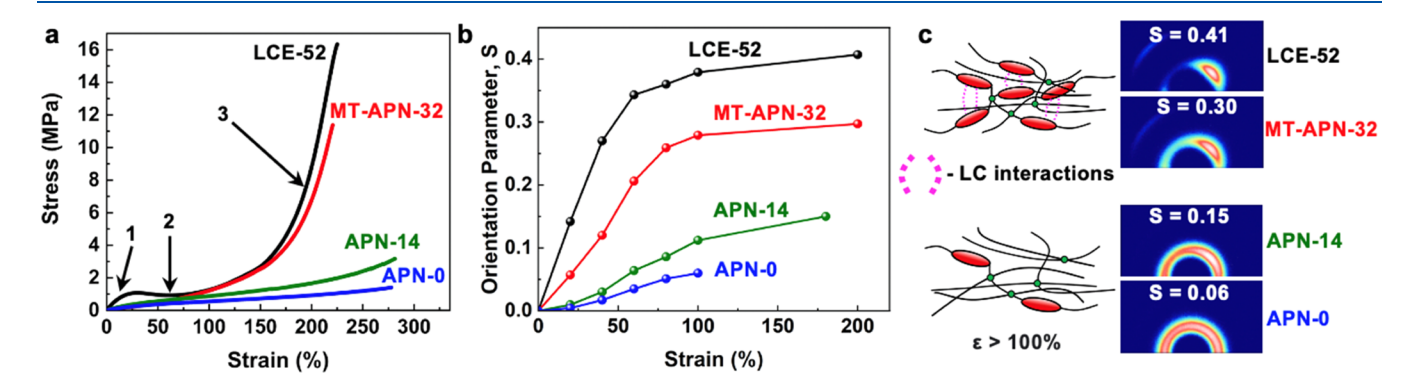


Figure 2. (a) Stress—strain response of the polymer networks prepared with 0–52 mol% LC. (b) Orientation parameter measured by 2-D WAXS for the same polymer networks as a function of strain. (c) Network illustrations of highly organized materials that develop enhanced LC interactions at high strains (LCE-52 and MT-APN-32) and materials that cannot organize and form LC phases (APN-14 and APN-0). These are accompanied by WAXS diffraction patterns at maximum elongation for each material and their measured orientation parameters (S).

coupling of deformation and order similarly to LCE-52 (Figure 2c, top left). Reducing the concentration of C6M (or more broadly, liquid crystalline units) in samples with comparatively low concentrations naturally limits the proximity and capacity of the mesogens to interact with each other, thus resulting in a weaker coupling of deformation and order (Figure 2c, bottom left). Due to this weaker coupling, APN-14, despite being composed of a small amount of LC content, does not undergo an MT phase transition upon deformation and overall is more similar in its behavior and properties to a purely amorphous polymer such as APN-0.

With these compositional differences established, we now consider whether the MT phase transition, such as that in MT-APN-32, is thermotropic (e.g., order depends on the temperature). Conventional elastomers are naturally temperature-dependent and stiffen with an increased temperature. Conversely, prior study of PD-LCE demonstrates that these materials soften with increased temperature. To better understand the similarities and differences between LCE and APN, we measured the modulus of these materials across a range of temperatures (Figure 3a). The modulus values were

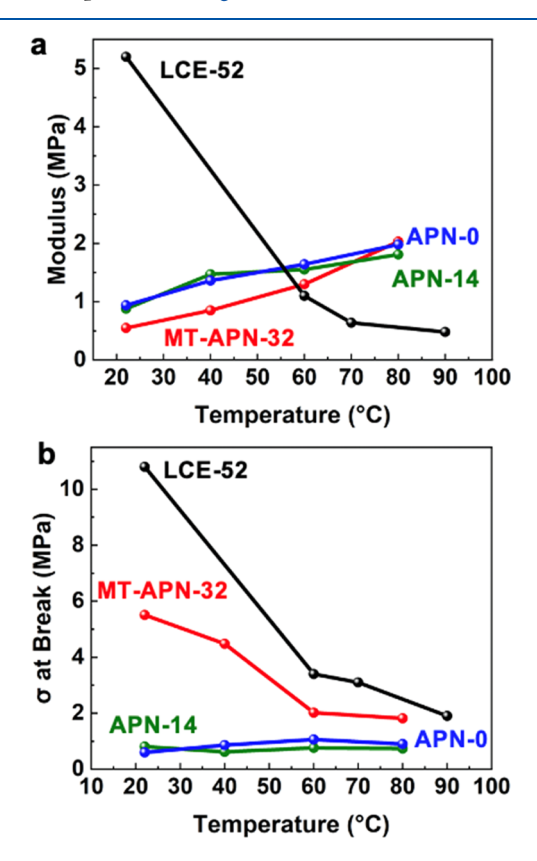


Figure 3. (a) Modulus as a function of the temperature of polymer networks prepared with 0–52 mol% LC. (b) Stress at break as a function of temperature.

taken from the slope of the linear elastic regime of the stress-strain curves. As evident in Figure 3a, increasing temperature results in an increase in the modulus for APN-0, APN-14, and MT-APN-32 and a decrease in the modulus for LCE-52. We note that although MT-APN-32 shares some mechanical features (described above) with LCE-52, in this context, the amorphous character of the APN-32 dominates its initial thermomechanical response (i.e., the modulus). This makes sense in that the modulus is taken within the first 10% of strain

when each material is still in the linear elastic region, and the embedded mesogens in MT-APN-32 may not have formed a well-organized LC phase (e.g., S = 0.06 at 20% strain for MT-APN-32, Supporting Information (SI) Figure 2). This contrasts with LCE-52 where an LC phase is present upon preparation and at all points of deformation. LCE-52 initially has a modulus much higher than that of all APN formulations. As with prior reports, LCE-52 materials soften dramatically (modulus decreases over 10x) to nearly 4x lower than the APN formulations by 90 °C. This effect is attributable to the disruption in LC mesogen intermolecular interactions at temperatures close to $T_{\rm NI}$. The ruggedness of the materials, illustrated here by stress at break, was also characterized as a function of temperature (Figure 3b). Increasing the temperature reduces the magnitude of the stress value at break for both LCE-52 and MT-APN-32, whereas it does not affect the values of APN-14 and APN-0. These data may indicate that the alignment mechanism of these materials may contribute to strengthening of the materials.

Conceptually, an MT-APN is analogous to a PD-LCE heated above its $T_{\rm NI}$. To illustrate this parallel, LCE-52 and MT-APN-32 were subjected to deformation across a range of temperatures. Tensile tests as a function of temperature for LCE-52 are shown in Figure 4a and for MT-APN-32 in Figure 4b (similar studies were also conducted for APN-14 and APN-0 and these data are shown in Figure S3a and S3b, respectively). At temperatures below the $T_{\rm NI}$ (22 and 70°C) of LCE-52, the material exhibits a soft elastic plateau (emphasized in the inset image of Figure 4a for 70°C) followed by strain hardening. Above $T_{
m NI}$, the deformation of LCE-52 changes, and a soft elastic plateau is no longer evident. Generally, the tensile deformation is very similar to that of the MT-APN-32 material at room temperature (22°C). Under these conditions, we expect the elevated temperature to disrupt the interactions between network-embedded mesogens in LCE-52 and results in more linear tensile responses with lower strains and stresses at break. Figure 4c directly compares the tensile response of MT-APN-32 at 22°C against that of LCE-52 at 105° C (just above the $T_{\rm NI}$ of 100° C for this material). At this temperature, it is apparent that LCE-52 is no longer in an LC phase such that its tensile response is comparable to that of MT-APN-32 at 22°C. Overall, a thermally induced isotropic PD-LCE network is mechanically similar to an MT-APN network. Both network types will experience a mechanically induced phase transition upon perturbation with mechanical strain from their isotropic states, regardless of whether those states occur due to formulation approaches (MT-APN materials) or thermal conditions (PD-LCE materials).

The orientation of these materials was assessed in two conditions: (i) at isostrain and (ii) at isoforce. Isostrain measurements for LCE-52 are reported in Figure 5a. As evident in Figure 5a-i, upon deformation to 100% strain, LCE-52 achieves an expected value of the orientation parameter for the nematic phase of 0.38. Upon heating this material to 110° C, again at 100% isostrain, the material retains this orientation (Figure 5a-ii). We considered whether the mechanical deformation of LCE-52 could effectively shift its $T_{\rm NI}$. Accordingly, we measured the isostrain orientation parameter of LCE-52 up to 250°C. These data, shown in Figure S5 as a function of temperature, indicate that LCE-52 at 100% strain retains orientation values exceeding 0.34. This association is confirmed in isostrain measurements collected with polarized optical microscopy, shown in Figure 5a-iii and

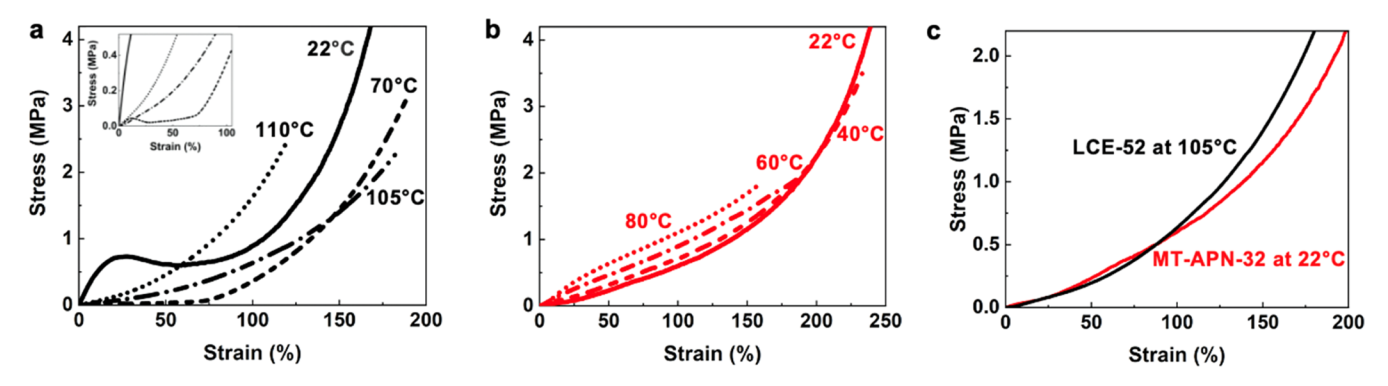


Figure 4. (a) Stress—strain responses of LCE-52 at varying temperatures. At room temperature, this material is an LCE in polydomain orientation. Upon heating, the material loses order, which affects the mechanical response to deformation. Inset highlights the soft elastic plateau still present at 70°C. (b) Stress—strain responses of MT-APN-32 at varying temperatures. LC interactions are disrupted at higher temperatures, which affects the deformation behavior. (c) Comparison of the stress—strain response of MT-APN-32 at room temperature and LCE-52 at 105°C.

Figure 5a-iv. Birefringence is evident at room temperature and 0% strain for LCE-52 when viewed under crossed polarizers (Figure 5a-iii). When LCE-52 is then taken to 100% strain at room temperature, a birefringence pattern is seen that corresponds to an aligned LCE (Figure S4a). Once again, upon heating to 110°C at 100% strain, LCE-52 retains its alignment as seen in its birefringence (Figure 5a-iv). Similarly, the MT-APN-32 material, when subjected to 100% strain, exhibits an orientation parameter of 0.28 (Figure 5b-i) that does not change upon heating (Figure 5b-ii, at 60°C). Again, this is also confirmed with imaging via polarized optical microscopy. Consistent with classic amorphous polymers, MT-APN-32 does not display any birefringence at room temperature and 0% strain (Figure 5b-iii) since the mechanically induced LC phase change has yet to be induced. When deformed to 100% strain at room temperature, MT-APN-32 shows a bright birefringence pattern (Figure S4b). At an elevated temperature and strain, MT-APN-32 maintains its strong birefringence, very similar to LCE-52 when it is aligned (Figure 5b-iv). Even at elevated temperatures, LCE-52 and MT-APN-32 retain their orientation and alignment as evidenced in their orientation parameters and birefringence patterns.

From these data, it is questionable whether the MT phase transition is thermotropic. However, we also subjected these representative materials to similar orientation parameter measurements collected under isoforce conditions. The isoforce orientation parameter values of LCE-52, MT-APN-32, and APN-14 are plotted against temperature in Figure 5c. In these experiments, each sample was fixed at one end, and a 20 g weight was attached at the other. This experimental setup was chosen so that the samples are in tension at room temperature but could then respond to increasing temperature. This setup mimics the classic LCE actuation demonstration done by Finkelmann.⁸ As with the prior measurements, the magnitude of the orientation parameter scales with the degree of liquid crystalline content. Upon heating, LCE-52 and MT-APN-32 undergo a significant change in orientation. At elevated temperatures, all three samples retain an orientation parameter of 0.1, which is likely attributable to the residual order associated with the load. These data indicate that the MT phase transition in MT-APN samples is thermotropic under isoforce conditions.

Accordingly, we conclude by examining the thermomechanical response of these materials in isoforce (Figure 6). Upon

heating, all four samples change length along the loading direction. Comparatively, the deformation of LCE-52 is the most significant, reaching nearly 50% strain upon heating. The magnitude of the strain generated decreases with a decreasing liquid crystalline content. In comparing the deformation of the MT-APN and APN samples, it is clear that the LC content increases the amount of deformation. These data confirm the thermotropic measurements in Figure 5c, where the materials are clearly changing in orientation and ultimately this order—disorder transition, as in aligned LCEs, results in a commensurate change in length.

CONCLUSIONS

Amorphous polymer networks (APN) were prepared with a range of liquid crystalline (LC) contents by thiol-Michael addition. In compositions prepared with a moderate LC content, the materials exhibit a mechanotropic transition (MT-APN) associated with the alignment of the embedded LC mesogens to the direction of stretch. While the orientational order of both polydomain LCE and MT-APN does not change when subject to isostrain, they are thermotropic in isoforce conditions. The thermotropic response of these materials under isoforce conditions is observed as thermomechanical actuation (strain generation) upon heating. This work further elucidates the fundamental understanding of mechanotropic phase transitions in LC-containing polymer networks and will benefit ongoing and emerging functional explorations including elastocaloric and optical materials.

METHODS

Materials. 1,4-Bis-[4-(6-acryloyloxyhexyloxy)benzoyloxy]-2-methylbenzene (C6M) was purchased from Wilshire Technologies (Princeton, NJ). Bisphenol A ethoxylate diacrylate (BPAEDA), 1,6 hexanedithiol (HDT), dipropylamine (DPA), and 4-methoxyphenol (MEHQ) were purchased from Sigma-Aldrich (St. Louis, MO). Omnirad 819 was purchased from iGM Resins (Charlotte, NC). All chemicals were used as received.

Polymer Network Synthesis. C6M, BPADA, Omnirad 819, and MEHQ were weighed and mixed in a vial. The ratio of C6M to BPAEDA was adjusted to control the amount of liquid crystalline content present in each material. The LC content was measured by mole percent. Four formulations were prepared with 52, 32, 14, and 0 mol% LC content. The compositions included 2 wt% Omnirad 819 (photoinitiator) and 1 wt% MEHQ (radical inhibitor). After the mixture was melted, HDT and DPA were added. HDT concentration was held constant at a mole ratio of 1.0:0.85 acrylate and thiol functional groups. DPA was added at 1 wt%. The compositions were

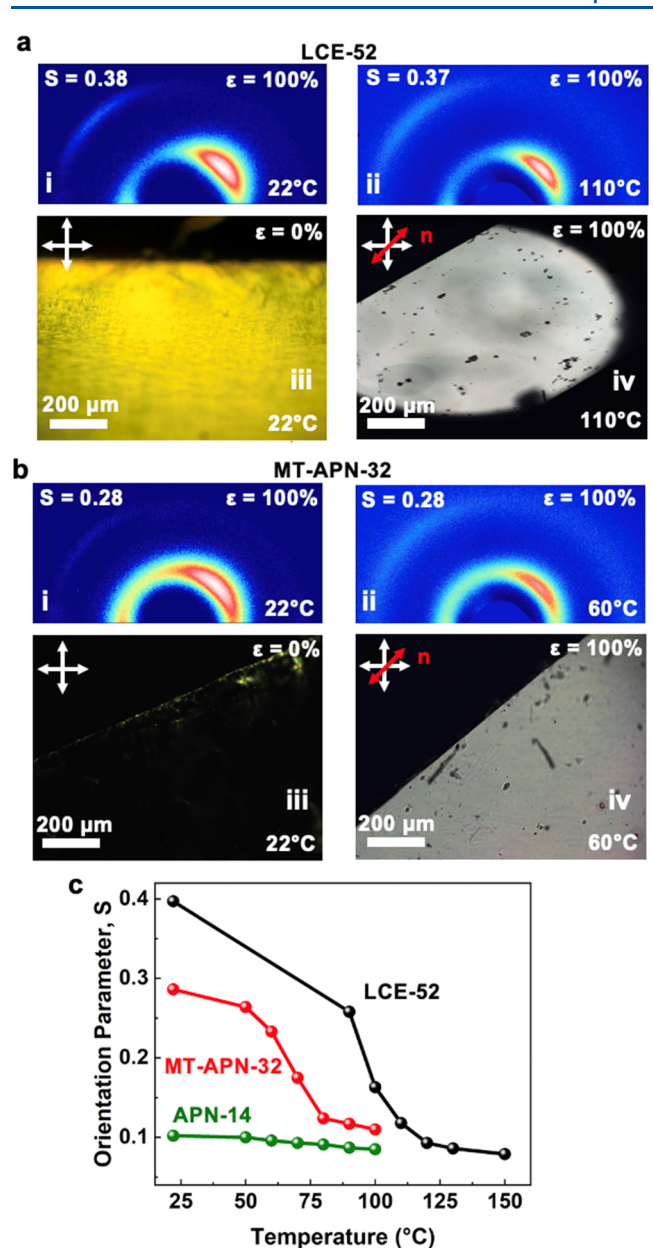


Figure 5. (a) WAXS patterns (i–ii) and POM images (iii–iv) of LCE-52 at varying strain and temperature conditions, (b) WAXS patterns and POM images of MT-APN-32 at varying strain and temperature conditions, and (c) isoforce orientation parameters calculated as a function of temperature for thermally actuated samples.

vigorously mixed by vortex mixing to ensure homogeneity. Subsequently, the formulation was drawn by pipet and cast onto heated glass slides. The formulations were sandwiched using another glass slide. 100 μ m spacers were added to regulate the thickness. The materials were first subject to thiol-Michael oligomerization at 100°C for 3 h. Thereafter, each formulation was polymerized, again at 100°C, by irradiation to 50 mW/cm² of 405 nm light for 5 min on each side. After polymerization, each material was cooled overnight before harvesting. The measured gel fractions for all materials ranged from 94 to 96%.

Characterization. Thermal analysis was undertaken with differential scanning calorimetry (DSC 2500-TA Instruments). The materials were subject to a heat-cool-heat cycle at 10°C/min (heating) and 5°C/min (cooling). Transition temperatures are reported from the second heating cycle. Mechanical properties and actuation response were measured by dynamic mechanical analysis

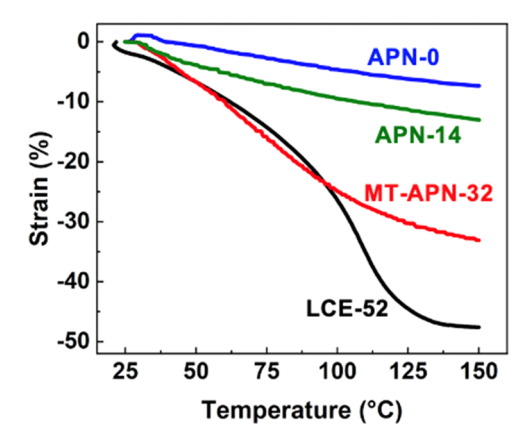


Figure 6. Isoforce actuation behavior as a function of temperature of all prepared polymer networks.

(DMA 850-TA Instruments). Unless noted, tensile deformation was conducted at T_g + 20°C to minimize the contributions of slight differences in the glass transition temperature. All rate-dependent tensile measurements were collected at 10% strain/min. The materials were deformed until failure. The thermomechanical actuation of the materials was examined under load. The materials were first deformed to 100% strain and held at a constant low force. The temperature was increased from room temperature to 150°C. For all DMA tests, strips of material were cut with approximate dimensions 20 mm long, 2 mm wide, and 100 µm thick. Polarized optical microscopy (POM) was utilized to assess the orientation of the materials before and during deformation, as a function of temperature. The temperature was controlled by an Instec heating stage. The materials were deformed with a custom-made tensile device. Strains were measured with calipers. Procedurally, we measured the starting length and then the length to deformation. Each sample was equilibrated at the specified temperature for several minutes before any images were taken to reduce any errors on the sample temperature. Orientation was quantified with wide-angle X-ray scattering (WAXS) on beamline 5-ID-D at the Advanced Photon Source located at Argonne National Laboratory. Each scan consisted of a 1-s X-ray exposure with an energy of 17 keV. The strain was controlled using an Instron servohydraulic tensile stage. The rate of strain was held at 10%/min with measurements taken every 20% strain until material failure. For experiments involving temperature and strain, a modular force stage (MFS-Linkam) was used. Each material was pulled to 100% strain and measurements were taken as a function of temperature. For the second set of WAXS experiments, a Xenocs Xeuss 3.0 was used, and scans consisted of a 120 s X-ray exposure with an energy of 8 keV and a sample to detector distance of 43.5 mm. For experiments where tension is held constant, samples are fixed at both ends while the temperature is increased, and scans are taken at specified temperatures. For actuation experiments, samples are held fixed at one end and then a 20 g weight is suspended from the bottom, allowing them to respond to increasing temperature. We ensured that the sample was in constant contact with the heating element to ensure accuracy in these experiments.

ASSOCIATED CONTENT

Data Availability Statement

Data is available on request from the authors.

Supporting Information

The Supporting Information is available free of charge at https://pubs.acs.org/doi/10.1021/acs.macromol.3c01869.

Additional characterization of prepared materials by DSC, POM, WAXS, and tensile testing (PDF)

AUTHOR INFORMATION

Corresponding Author

Timothy J. White — Department of Chemical and Biological Engineering, University of Colorado, Boulder, Colorado 80309, United States; Materials Science and Engineering Program, University of Colorado, Boulder, Colorado 80309, United States; orcid.org/0000-0001-8006-7173; Email: tim.white@colorado.edu

Authors

- Jeremy A. Herman Department of Chemical and Biological Engineering, University of Colorado, Boulder, Colorado 80309, United States
- Jonathan D. Hoang Materials Science and Engineering Program, University of Colorado, Boulder, Colorado 80309, United States
- Joselle M. McCracken Department of Chemical and Biological Engineering, University of Colorado, Boulder, Colorado 80309, United States; orcid.org/0000-0002-0411-3542

Complete contact information is available at: https://pubs.acs.org/10.1021/acs.macromol.3c01869

Notes

The authors declare no competing financial interest.

ACKNOWLEDGMENTS

This work was supported in part by the Petroleum Research Fund of the American Chemical Society. J.A.H. acknowledges support from the National Science Foundation via a Graduate Research Fellowship. The authors acknowledge beamline 5-ID-D at Argonne National Laboratory for their help in collecting WAXS patterns and for the use of their facilities. The Xenocs Xeuss 3.0 was purchased through funding from a Defense University Research Instrumentation Program under Grant Number N00014-22-1-2361.

REFERENCES

- (1) Brannum, M. T.; Steele, A. M.; Venetos, M. C.; Korley, L. S. T. J.; Wnek, G. E.; White, T. J. Light Control with Liquid Crystalline Elastomers. *Adv. Opt. Mater.* **2019**, *7* (6), No. 1801683.
- (2) Schlafmann, K. R.; White, T. J. Retention and Deformation of the Blue Phases in Liquid Crystalline Elastomers. *Nat. Commun.* **2021**, 12, No. 4916.
- (3) Shang, Y.; Wang, J.; Ikeda, T.; Jiang, L. Bio-Inspired Liquid Crystal Actuator Materials. J. Mater. Chem. C 2019, 7 (12), 3413–3428
- (4) Auguste, A. D.; Ward, J. W.; Hardin, J. O.; Kowalski, B. A.; Guin, T. C.; Berrigan, J. D.; White, T. J. Enabling and Localizing Omnidirectional Nonlinear Deformation in Liquid Crystalline Elastomers. *Adv. Mater.* **2018**, *30* (35), No. 1802438.
- (5) Kim, H.; Gibson, J.; Maeng, J.; Saed, M. O.; Pimentel, K.; Rihani, R. T.; Pancrazio, J. J.; Georgakopoulos, S. V.; Ware, T. H. Responsive, 3D Electronics Enabled by Liquid Crystal Elastomer Substrates. ACS Appl. Mater. Interfaces 2019, 11 (21), 19506—19513.
- (6) Shaha, R. K.; Merkel, D. R.; Anderson, M. P.; Devereaux, E. J.; Patel, R. R.; Torbati, A. H.; Willett, N.; Yakacki, C. M.; Frick, C. P. Biocompatible Liquid-Crystal Elastomers Mimic the Intervertebral Disc. J. Mech. Behav. Biomed. Mater. 2020, 107, No. 103757.
- (7) Martella, D.; Parmeggiani, C. Advances in Cell Scaffolds for Tissue Engineering: The Value of Liquid Crystalline Elastomers. *Chem. Eur. J.* **2018**, 24 (47), 12206–12220.
- (8) White, T. J.; Broer, D. J. Programmable and Adaptive Mechanics with Liquid Crystal Polymer Networks and Elastomers. *Nat. Mater.* **2015**, *14*, 1087–1098.

- (9) Wang, M.; He, L.; Zorba, S.; Yin, Y. Magnetically Actuated Liquid Crystals. *Nano Lett.* **2014**, *14* (7), 3966–3971.
- (10) Winkler, M.; Kaiser, A.; Krause, S.; Finkelmann, H.; Schmidt, A. M. Liquid Crystal Elastomers with Magnetic Actuation. *Macromol. Symp.* **2010**, 291–292 (1), 186–192.
- (11) Fowler, H. E.; Rothemund, P.; Keplinger, C.; White, T. J. Liquid Crystal Elastomers with Enhanced Directional Actuation to Electric Fields. *Adv. Mater.* **2021**, 33 (43), No. 2103806.
- (12) Wermter, H.; Finkelmann, H. Liquid Crystalline Elastomers as Artificial Muscles. *e-Polym.* **2001**, *1* (1), No. 111, DOI: 10.1515/epoly.2001.1.1.111.
- (13) Ohm, C.; Brehmer, M.; Zentel, R.; Ohm, C.; Brehmer, M.; Zentel, R. Liquid Crystalline Elastomers as Actuators and Sensors. *Adv. Mater.* **2010**, 22 (31), 3366–3387.
- (14) Serak, S.; Tabiryan, N.; Vergara, R.; White, T. J.; Vaia, R. A.; Bunning, T. J. Liquid Crystalline Polymer Cantilever Oscillators Fueled by Light. *Soft Matter* **2010**, *6*, 779–783.
- (15) Donovan, B. R.; Matavulj, V. M.; Ahn, S. kyun.; Guin, T.; White, T. J. All-Optical Control of Shape. *Adv. Mater.* **2019**, *31* (2), No. 1805750.
- (16) Herbert, K. M.; Fowler, H. E.; McCracken, J. M.; Schlafmann, K. R.; Koch, J. A.; White, T. J. Synthesis and Alignment of Liquid Crystalline Elastomers. *Nat. Rev. Mater.* **2022**, *7*, 23–38.
- (17) Küpfer, J.; Finkelmann, H. Nematic Liquid Single Crystal Elastomers. *Makromol. Chem., Rapid Commun.* **1991**, *12* (12), 717–726, DOI: 10.1002/marc.1991.030121211.
- (18) Yakacki, C. M.; Saed, M.; Nair, D. P.; Gong, T.; Reed, S. M.; Bowman, C. N. Tailorable and Programmable Liquid-Crystalline Elastomers Using a Two-Stage Thiol—Acrylate Reaction. *RSC Adv.* **2015**, *5* (25), 18997—19001.
- (19) Ware, T. H.; McConney, M. E.; Wie, J. J.; Tondiglia, V. P.; White, T. J. Voxelated Liquid Crystal Elastomers. *Science* **2015**, 347 (6225), 982–984.
- (20) Kowalski, B. A.; Guin, T. C.; Auguste, A. D.; Godman, N. P.; White, T. J. Pixelated Polymers: Directed Self Assembly of Liquid Crystalline Polymer Networks. *ACS Macro Lett.* **2017**, *6* (4), 436–441.
- (21) Ambulo, C. P.; Burroughs, J. J.; Boothby, J. M.; Kim, H.; Ravi Shankar, M.; Ware, T. H. Four-Dimensional Printing of Liquid Crystal Elastomers. *ACS Appl. Mater. Interfaces* **2017**, 9 (42), 37332–37339.
- (22) Saed, M. O.; Ambulo, C. P.; Kim, H.; De, R.; Raval, V.; Searles, K.; Siddiqui, D. A.; Cue, J. M. O.; Stefan, M. C.; Shankar, M. R.; Ware, T. H. Molecularly-Engineered, 4D-Printed Liquid Crystal Elastomer Actuators. *Adv. Funct. Mater.* **2019**, 29 (3), No. 1806412.
- (23) Brannum, M. T.; Auguste, A. D.; Donovan, B. R.; Godman, N. P.; Matavulj, V. M.; Steele, A. M.; J Korley, L. T.; Wnek, G. E.; White, T. J. Deformation and Elastic Recovery of Acrylate-Based Liquid Crystalline Elastomers. *Macromolecules* **2019**, 52 (21), 8248–8255.
- (24) Donovan, B. R.; Fowler, H. E.; Matavulj, V. M.; White, T. J. Mechanotropic Elastomers. *Angew. Chem., Int. Ed.* **2019**, 58 (39), 13744–13748.
- (25) Urayama, K.; Mashita, R.; Kobayashi, I.; Takigawa, T. Stretching-Induced Director Rotation in Thin Films of Liquid Crystal Elastomers with Homeotropic Alignment. *Macromolecules* **2007**, *40* (21), 7665–7670.
- (26) Clarke, S. M.; Terentjev, E. M.; Kundler, I.; Finkelmann, H. Texture Evolution during the Polydomain-Monodomain Transition in Nematic Elastomers. *Macromolecules* **1998**, *31* (15), 4862–4872.
- (27) Urayama, K.; Kohmon, E.; Kojima, M.; Takigawa, T. Polydomain-Monodomain Transition of Randomly Disordered Nematic Elastomers with Different Cross-Linking Histories. *Macromolecules* **2009**, 42 (12), 4084–4089.
- (28) Shaha, R. K.; Torbati, A. H.; Frick, C. P. Body-Temperature Shape-Shifting Liquid Crystal Elastomers. *J. Appl. Polym. Sci.* **2021**, 138 (14), No. 50136.
- (29) Barnes, M.; Cetinkaya, S.; Ajnsztajn, A.; Verduzco, R. Understanding the Effect of Liquid Crystal Content on the Phase

Behavior and Mechanical Properties of Liquid Crystal Elastomers. *Soft Matter* **2022**, *18* (27), 5074–5081.

- (30) Yoon, H.-H.; Kim, D.-Y.; Jeong, K.-U.; Ahn, S.-K. Surface Aligned Main-Chain Liquid Crystalline Elastomers: Tailored Properties by the Choice of Amine Chain Extenders. *Macromolecules* **2018**, *51* (3), 1141–1149.
- (31) McCracken, J. M.; Donovan, B. R.; Lynch, K. M.; White, T. J. Molecular Engineering of Mesogenic Constituents Within Liquid Crystalline Elastomers to Sharpen Thermotropic Actuation. *Adv. Funct. Mater.* **2021**, *31* (16), No. 2100564, DOI: 10.1002/adfm.202100564.
- (32) Bauman, G. E.; McCracken, J. M.; White, T. J. Actuation of Liquid Crystalline Elastomers at or Below Ambient Temperature. *Angew. Chem., Int. Ed.* **2022**, *61* (28), No. e202202577.
- (33) Cong, D.; Xiong, W.; Planes, A.; Ren, Y.; Mañosa, L.; Cao, P.; Nie, Z.; Sun, X.; Yang, Z.; Hong, X.; Wang, Y. Colossal Elastocaloric Effect in Ferroelastic Ni-Mn-Ti Alloys. *Phys. Rev. Lett.* **2019**, *122* (7), No. 255703, DOI: 10.1103/PhysRevLett.122.255703.
- (34) Bonnot, E.; Romero, R.; Mañosa, L.; Vives, E.; Planes, A. Elastocaloric Effect Associated with the Martensitic Transition in Shape-Memory Alloys. *Phys. Rev. Lett.* **2008**, *100* (12), No. 125901.
- (35) Pataky, G. J.; Ertekin, E.; Sehitoglu, H. Elastocaloric Cooling Potential of NiTi, Ni2FeGa, and CoNiAl. *Acta Mater.* **2015**, *96*, 420–427.
- (36) Guyomar, D.; Li, Y.; Sebald, G.; Cottinet, P. J.; Ducharne, B.; Capsal, J. F. Elastocaloric Modeling of Natural Rubber. *Appl. Therm. Eng.* **2013**, 57 (1–2), 33–38.
- (37) Xie, Z.; Sebald, G.; Guyomar, D. Elastocaloric Effect Dependence on Pre-Elongation in Natural Rubber. *Appl. Phys. Lett.* **2015**, *107* (8), No. 081905.
- (38) Greibich, F.; Schwödiauer, R.; Mao, G.; Wirthl, D.; Drack, M.; Baumgartner, R.; Kogler, A.; Stadlbauer, J.; Bauer, S.; Arnold, N.; Kaltenbrunner, M. Elastocaloric Heat Pump with Specific Cooling Power of 20.9 W g⁻¹ Exploiting Snap-through Instability and Strain-Induced Crystallization. *Nat. Energy* **2021**, *6* (3), 260–267.
- (39) Koch, J. A.; Herman, J. A.; White, T. J. Elastocaloric Effect in Amorphous Polymer Networks Undergoing Mechanotropic Phase Transitions. *Phys. Rev. Mater.* **2021**, *5* (6), No. L062401.
- (40) Mistry, D.; Nikkhou, M.; Raistrick, T.; Hussain, M.; Jull, E. I. L.; Baker, D. L.; Gleeson, H. F. Isotropic Liquid Crystal Elastomers as Exceptional Photoelastic Strain Sensors. *Macromolecules* **2020**, *53* (10), 3709–3718.

